Ultra Wideband Gated Step Frequency Ground Penetrating Radar

Mats Jørgen Øyan, Svein-Erik Hamran, Leif Hanssen, Tor Berger and Dirk Plettemeier

***Abstract*—We describe a prototype ultra wideband radar. We show how the system was designed and the hardware developed for the radar prototype. Waveform generation, radar parameters and signal processing for the stepped frequency waveform are discussed. The radar operates from 500 MHz to 3 GHz with a nominal resolution of 6 cm in air. The advantage of the stepped frequency approach over an impulse radar is better matching between the transmitted waveform and the receiver. We use range gating to improve the system dynamic range. The advantages are illustrated with lab measurements and field measurements from glacial ice and permafrost on Svalbard showing penetration depths of 11 m. Antennas which do not require contact with the ground were developed and used in the experiments.**

I. Introduction

WE discuss a prototype for the WISDOM[1] ground penetrating radar (GPR), which has been selected for the European Space Agency's (ESA) first mission in the Aurora programme the ExoMars mission [1]. The mission is intended to search for proof of life, past or present. One of the places to look for this is in sub-surface permafrost or ice. The ExoMars descent module will contain a mobile rover upon which WISDOM will be mounted along with a drill. The rover drill can take samples, but drilling is energy-expensive and the drill wears down, limiting its use. Knowing where to drill strongly raises the probability of getting interesting samples. The WISDOM radar is intended to map the structures of the shallow sub-surface, an ability which adds greatly to the usefulness of the drill. To serve these requirements, a high resolution radar which penetrates 3 m into the Martian soil is needed. To reduce the risk of the rover getting caught on obstructions, the antennas must be raised above ground. The direct coupling between antennas needs to be reduced for improved system dynamic range and the power usage needs to be minimized because of the limited power budget of the rover.

Ultra wideband (UWB) radars have high fractional bandwidth [2]. One application is GPR, used to locate buried objects and interfaces such as mine detection [3] and glacier mapping [4]. GPR is often used in close proximity to the ground, but can also be airborne or satellite based. Experiments on soil simulating the martian sub-surface show that penetration depth decreases with increased frequency [5]. However, low frequencies means large antennas, which are heavy and difficult to mount on a small rover.

M.J. Øyan, S.-E. Hamran, L. Hanssen and T. Berger are with the Norwegian Defence Research Establishment, e-mail: Mats-Jorgen.Oyan@ffi.no.

D. Plettemeier is with the Technische Universitt Dresden.

[1]Water Ice and Subsurface Deposit Observations on Mars

Impulse-like radar is a common choice as a waveform in GPR systems [6] [7]. An impulse radar works in the time-domain and obtains high range resolution by transmitting a wideband impulse. This method requires high sampling frequencies, and the equivalent time sampling technique [8] is often used above 100 MHz to reconstruct the traces. Creating the impulse is easy, but the sampling technique means that much of the energy transmitted and reflected goes to waste. Frequency Modulated Continuous Wave (FMCW) is also used for GPR, and for through-the-wall applications [9] and synthetic aperture radar [10]. FMCW systems work by transmitting a repetitive waveform with increasing or decreasing frequency. The frequency response is later synthesized to an impulse. UWB FMCW systems require an extremely linear sweep, which can be difficult to create, and sampling of a beat frequency.

A different approach is the step frequency continuous wave (SFCW) radar, which synthesises an impulse from a finite spectrum. There are several advantages in using a SFCW system. Generating one single narrowband signal at a time is simple compared to generating the linear FMCW sweep. Using only a low-frequency oscillating source and a programmable phase locked loop (PLL), one can create a step frequency waveform generator. This requires simpler hardware than for the FMCW radar. If we ignore target movement relative to the radar, the signal sampled by the receiver is a DC signal containing noise. This reduces the sampling requirements, given by Nyquist, to two times the bandwidth of the intermediate frequency (IF) low pass filter in the receiver. Disregarding the setup time, no the transmitted energy is lost. This is an important feature for a system going to Mars where energy reserves are limited. The disadvantage of SFCW compared to FMCW is the settling time required for the PLL to obtain lock for each frequency. Simple hardware is considered more important than the maximum pulse repetition frequency for the WISDOM radar. Step frequency radar have been used as SAR systems [11] [12] and GPR [3].

In FMCW and SFCW radars, the receiver and transmitter are on at the same time. The direct wave between antennas may be the strongest signal, limiting the system dynamic range. By using range gating, this signal can be reduced [13]. This allows us to transmit more power, improving the system dynamic range [14] and effectively enabling the radar to see weaker targets deeper in the ground.

The Martian sub-surface has been analyzed by satellite based ground penetrating radars such as the Mars Advanced Radar for Sub-surface and Ionosphere Sounding (MARSIS) and The Mars Shallow Radar Sounder (SHARAD). These

Dette er en postprint-versjon / This is a postprint version.
DOI til publisert versjon / DOI to published version: 10.1109/TGRS.2011.2160069

systems have a vertical resolution of 50-100 m and 10-20 m with penetration up to 3 km and 200 m into the Mars sub-surface respectively [15]. WISDOM is planned to be the first mobile radar on the surface of Mars.

In order to provide high-resolution data of the upper three meters of the Martian ground, WISDOM needs low center frequency for penetration and high bandwidth for resolution. We believed that the SFCW waveform combined with gating to reduce the direct wave and surface reflection is an optimal combination for this type of radar.

Our objective was to make a prototype of a gated step frequency radar with miniaturized components for use in GPR applications. We discuss the benefits of gating to remove the direct wave and surface reflection for a stand-off SFCW radar. We demonstrate high resolution and penetration in permafrost and ground ice, as required for the WISDOM radar. The RF part of the radar is as close to the flight-version of the WISDOM radar as possible, and the control system reconfigurable to test different modes. We developed new antennas for the 500-3000 MHz frequency range. The flight version of the radar will be able to collect full polarimetric measurements, but the prototype discussed in this paper is single polarization only.

We start this paper by describing the step frequency waveform. We continue by introducing the hardware developed for the prototype, and we describe the signal processing needed to convert the radar data to the time domain. The prototype has two modes, CW and gated, which are discussed and compared. We summarize our radar parameters and their effects on the system and continue with the design and performance of the antennas developed for the WISDOM radar prototype. The radar was tested in the lab and in a field test on Svalbard. The results from these tests are presented, and finally, we give our conclusions.

II. Radar System

THE design parameters for the WISDOM radar are derived from the Instrument Information Package [16].

The rover drill is capable of drilling 2 m into the ground, and GPR data should be available to at least 3 m depth. The measurable range for the radar depends on two factors, all external parameters being equal: The signal to noise ratio (SNR) and the unambiguous range.

An unambiguous range that is too short, where distant reflectors are undersampled, will result in false, aliased reflections. Trace stacking over time or increased output power improve SNR. If the output power is increased, eventually the receiver may become saturated due to antenna coupling or strong reflectors. These problems can be handled by gating the radar.

The radar needs good range resolution, Δr, of a few centimeters to separate internal layers in the sub-surface. The quantity Δr is determined from the bandwidth B and the radar wave propagation speed v as

$$\Delta r = \frac{v}{2 \cdot B}. \tag{1}$$

A diagram of the radar is shown in fig. 1. The different parts will be discussed in this section.

A. Waveform

The WISDOM prototype samples in the frequency domain. Only one single frequency is transmitted at a time. Before sampling the received signal, the phase locked loop PLL2, shown in fig. 1, is allowed to obtain lock. The received signal will be at the same frequency as the transmitted, only with a phase shift. This phase shift results from the combined reflections of all the illuminated targets. Fig. 2 shows how the frequency changes as a function of time for the step frequency waveform. The detail in fig. 3 shows how three frequencies are set. The system first needs to be programmed and the PLL locked, which takes time, t_{su}, before sampling can begin. When M samples have been recorded, after $M \cdot t_s$, where $M = 10$, the radar changes the frequency by Δf. When the last frequency has been sampled, the frequency domain data for one complete radar trace has been collected and can be processed. A typical radar trace takes 50-100 ms to collect which means 10-20 traces per second.

The unambiguous range is given by the frequency step and is directly proportional to the number of frequencies sampled for a given bandwidth. The unambiguous time window is derived from the bandwidth B and number of frequencies N, such that

$$t_{ua} = \frac{N-1}{2 \cdot B}, \tag{2}$$

and should be chosen to be equal to or greater than the expected range of penetration into the sub-surface. This gives the number of frequencies for a given bandwidth.

B. Hardware

The radar circuitry is split between two printed circuit boards (PCB) as shown in fig. 4. The data collection/signal generation PCB, shown on the right hand side of fig. 4, and the RF PCB, on the left hand side of fig. 4, are connected and mounted in a waterproof case for field use. Power, USB and an optional encoder are connected to the case through external connectors. There are also SMA-connectors for the antennas and a system for mounting the radar on a fiberglass pole.

A microcontroller (labeled uC) mounted on the data collection/signal generation PCB controls all the programmable components, timing of the radar and communication with the computer through USB. The USB interface is a commercial module and USB 2.0 compatible, allowing up to 480Mb/s data transfer. Two direct digital synthesis (DDS) circuits generate two low frequency signals in the 0-30MHz range. One creates the SFCW waveform, while the other is routed through the delay circuits and used for gating as explained in section II-D. The analog to digital converter (ADC) is 16 bit and uses a 1MHz sampling clock. This gives a theoretical receiver dynamic range of 96.4dB. Samples from the ADC are buffered in a First-In-First-Out buffer (FIFO) and transferred to a computer through the USB interface.

The RF board contains all the microwave components. The phase locked loop on the top (Fig. 4 PLL1) receives a 10MHz signal from the data collection/signal generation PCB and creates a 8 GHz local oscillator (LO) signal. The PLL2 receives a reference signal from DDS1 and generates a

Dette er en postprint-versjon / This is a postprint version.
DOI til publisert versjon / DOI to published version: 10.1109/TGRS.2011.2160069

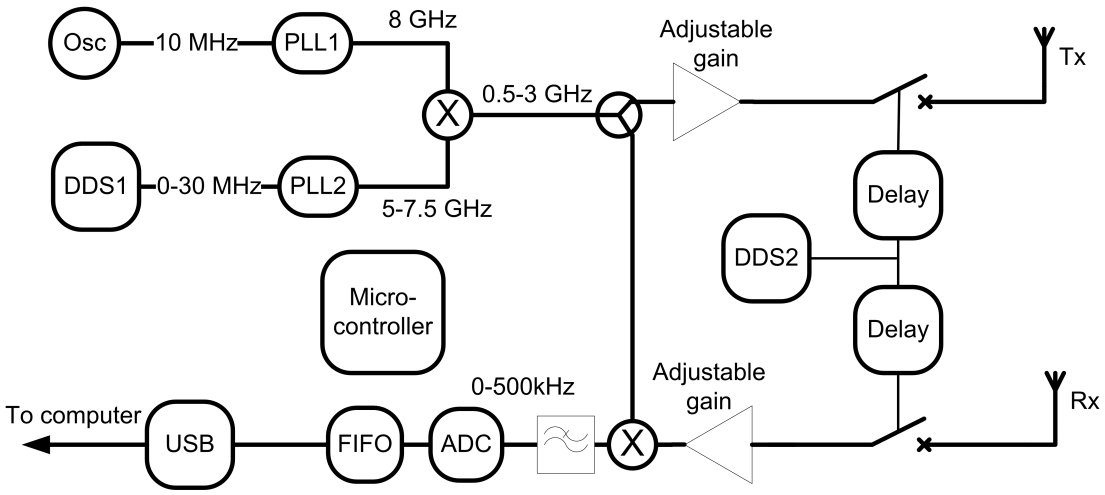

Fig. 1. Schematic diagram of the WISDOM prototype radar

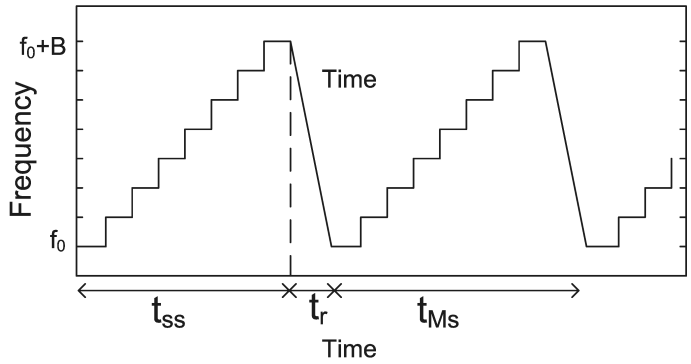

Fig. 2. The step frequency waveform which increases frequency in discrete steps until the bandwidth is covered. Then the frequency is reset to the start frequency and the process is repeated. t_{ss} is the time used to collect one trace and t_r is the reset time between traces. t_{Ms} the time it takes for each measurement relates to the pulse repetition frequency (PRF) as $PRF = 1/t_{Ms}$.

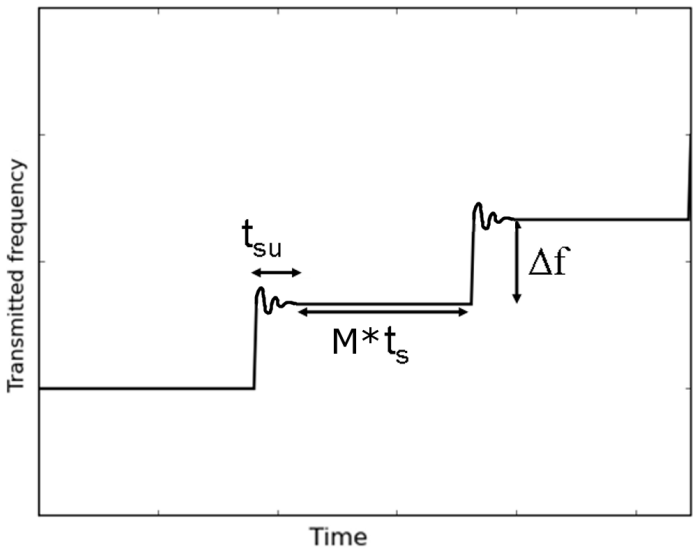

Fig. 3. Detailed view of the step frequency waveform. The setup delay (t_{su}) and time for sampling (Mt_s) is shown, as well as the change in frequency (Δf) between each measurement

signal between 5 and 7.5 GHz. The signal from the two PLLs are mixed and filtered, resulting in frequencies between 0.5-3 GHz. This signal is split, with one part being amplified with adjustable gain, gated and transmitted through the antenna. The gain is controlled by a programmable attenuator (0-31 dB) and the gates are controlled by the DDS. The Rx-chain is similar, with gating and adjustable gain before the received signal is mixed with the reference signal. The IF signal from the mixer is routed to the ADC on the low frequency board and sampled there.

C. Signal Processing

Ten samples are received for each frequency. This increases the integration time for each frequency, which makes the SFCW radar more energy efficient because the sampling time to settling time ratio increases [17]. The ten samples for each transmitted frequency are averaged into one sample by taking the sum and dividing it by ten. This effectively reduces the IF bandwidth and thereby reduces the thermal noise. With one sample for each frequency, a Blackman window function is applied to the data. We then place the samples correctly in the frequency domain. Since the first transmitted frequency is 500 MHz, we put zeros in place for the missing frequencies to get the correct phase of the compressed pulse. Zero padding is also added behind the data to interpolate the data in the time domain to increase the visual representation. We apply an inverse Fourier transform to bring the data into the time domain, and plot the real part to retain the phase information to make it easier to follow sub-surface interfaces.

When the traces have been transformed to time, the data are indistinguishable from a conventional impulse radar. The received traces are plotted consecutively in line and processed as a normal GPR profile. Processing may include background removal, adding gain, deconvolution and migration for example.

Dette er en postprint-versjon / This is a postprint version.
DOI til publisert versjon / DOI to published version: 10.1109/TGRS.2011.2160069

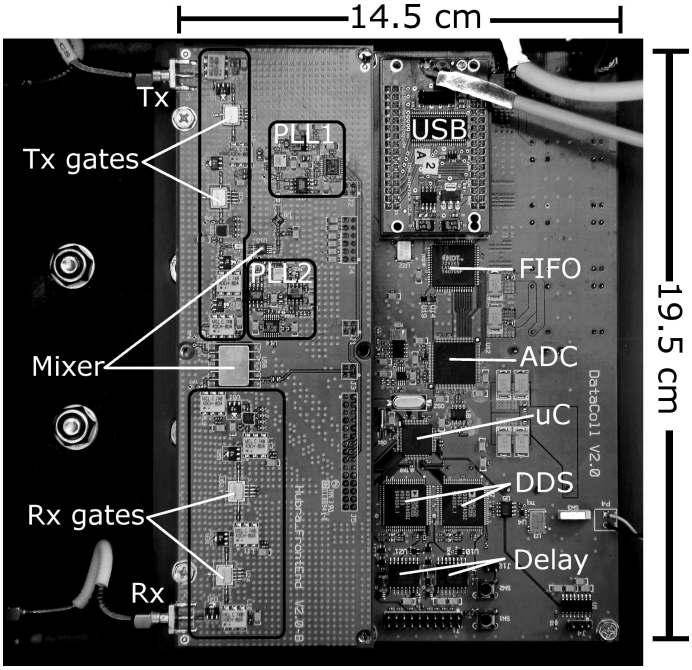

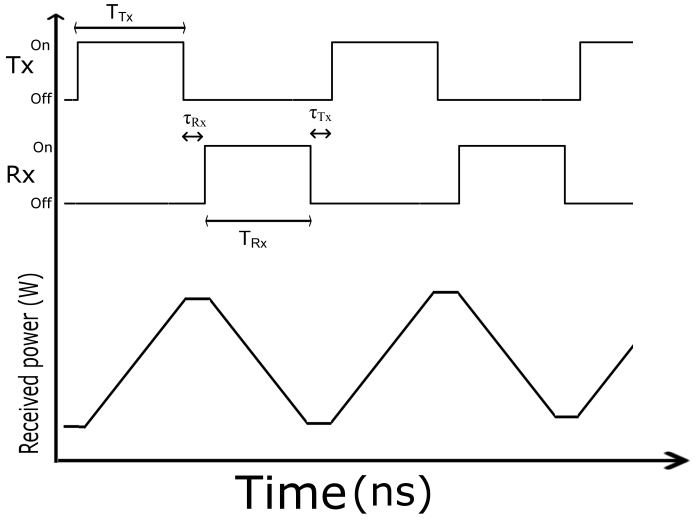

Fig. 5. The Tx and Rx gating signals with the tunable parameters, and the effect of gating window on received power as a function of time. The tunable delay symbols are defined in the text.

Fig. 4. WISDOM prototype PCBs. To the left is the RF-board with SMA antenna connectors. To the right is the data collection/signal generation board with USB and power connectors.

D. CW and Gating

The prototype supports two modes. In the continuous wave (CW) mode , both the transmitter and receiver chain are always turned on during recordings. This is simple to implement, but the disadvantage is a strong direct wave propagating from the transmitting to the receiving antenna. The transmitter power and receiver gain needs to be adjusted so the ADC is not saturated.

The gated step frequency mode uses a gating signal (fig. 5) to turn on and off the transmitter and receiver chain [13]. The gating signal is generated by DDS2, which allows for quick changes in the gating frequency from 0 Hz to 20 MHz, limited by the gates used. When the signal is gated, a small part of the waveform is transmitted from the antenna before the receiver is switched on. This means only a small fraction of the reflected signal from close targets will be collected at the receiver. For reflections at a distance of half the gating period from the radar, the whole transmitted wave will be received. Fig. 5 shows how the received power varies with distance from the radar due to gating. The sampled signal strength can be seen as a convolution of the transmitter- and receiver-gating signals. The result is a gating window with maximum attenuation at zero range, maximum signal strength at half the period of the gating frequency and maximum attenuation for reflections with a distance equal to the gating period. The whole area of interest is kept within the first gating window.

The tunable variables shown in fig. 5 are T_{Tx} and T_{Rx}. They are given by the gating frequency and the delays τ_{Tx} and τ_{Rx}, which can be controlled separately by two delay circuits. Targets close to the radar are attenuated because of the convolution, and the direct signal between antennas can be reduced or even removed by a combination of gating frequency and delay.

E. Parameters

The radar system is highly configurable. Most parameters can be set in software, allowing different configurations. However, most measurements have been taken with a default setup, as shown in Table I. The first transmitted frequency is 500 MHz, increasing in 3.33 MHz steps up to 3 GHz. These 751 frequencies gives us, from equation 2, an unambiguous range of 150 ns.

Programming a new frequency and letting the PLL lock takes 91 μs. The sampling frequency is 1 MHz and since 10 samples are taken for each frequency, sampling takes 10 μs. A complete trace takes (91 μ s + 10 μ s) $\cdot$ 751 = 75.851 ms, with approximately 13 traces per second.

The gating frequency we choose is 5.12 MHz. The period for this signal is about 195 ns, with the first gating zero outside the trace. No attenuation or delay in the gating signal is needed.

TABLE I
RADAR PARAMETERS

Center frequency	1.75 GHz
Bandwidth	2.5 GHz
Frequency steps	751
Samples pr frequency	10
t_{su}	91 μs
Gate frequency	5.12 MHz
Gate delay	0 ns
Tx attenuation	0-31 dB
Rx attenuation	0-31 dB
Distance/sample	20 cm
AD	16 bit
Sampling frequency	1 MHz
Transmitted power	$\approx 0dBm$

III. ANTENNAS

Dette er en postprint-versjon / This is a postprint version.
DOI til publisert versjon / DOI to published version: 10.1109/TGRS.2011.2160069

THE flight version of the WISDOM radar will be a full-polarimetric radar. Analysis of depolarization effects requires a full polarimetric antenna system working in the frequency range from 500 MHz to 3 GHz. The antenna design consists of two perpendicular linearly polarized transmitting antennas and two co- and cross-polar oriented antennas for reception [18]. Usually GPR antennas are placed on the ground or accommodated in a configuration close to the ground with respect to the wavelength. The antenna accommodation on the ExoMars requires a ground clearance of about 30 cm, which is equal to 3 wavelengths for the highest operating frequency. Taking into account that the antennas on the rover are not able to use the advantages of a near ground arrangement, the radiation pattern of each single antenna element has to accommodate scientific requirements, radiation coupling effects and electromagnetic compatibility requirements. The along-track pattern has to be wide to provide visibility of point reflectors over long distances. The cross-track path pattern should be narrow.

Requirements on planetary protection and constraints on mass and volume led to an antenna design that is based on Vivaldi structures. To realize the full polarimetric antenna system we combined perpendicularly oriented Vivaldi elements in each of the two dual polarized antennas. Both units are covered by a thin dielectric foil to protect against Martian dust. The overall size of a dual polarized antenna is less than 20 cm x 20 cm x 20 cm and the mass is less than 200 g. Despite the electrically small dimensions, the characteristic of the antenna gain versus frequency is smooth, starting from about 2 dBi at low frequencies up to about 9 dBi at higher frequencies. The return loss is less than -10 dB over the whole frequency range. The current prototype consists of novel glass and carbon fiber reinforced plastics.

IV. Results

WE have performed several tests in the lab and in the field on Svalbard. The laboratory test was to characterize the radar performance. The field test served as a possible Mars analog.

A. Lab Test

The step frequency technique relies on the transmitted frequencies having approximately the same power. We used a spectrum analyzer to measure the transmitting power whilst stepping through all frequencies, with the gating disabled. The resulting spectrum is shown in fig. 6. The average transmitted power was approximately 0 dBm, and the difference between 0.5 and 3 GHz is 12.8 dB. The Tx and Rx front ends use 5 Gali-49+ and one Gali-39+ amplifiers (Mini-Circuits). The difference in gain for 500 MHz and 3 GHz from the data sheet is respectively, approximately 0.5 dB and 4.7 dB. Combined for all amplifiers, the difference in gain between the lowest and highest frequency is 7.2 dB. The remaining 5.6 dB can be a result of higher attenuation in the circuit board and additional component loss for high frequencies. The variation in power does not change from pulse to pulse, and can be compensated in the window function applied to the data.

We tested the performance of the radar with delay cables connected as shown in fig. 7. The setup simulated four reflectors. The shortest cable was attenuated by 21 dB and simulated the direct wave between transmitting and receiving antenna with a delay of 10.7 ns. The air-ground interface reflection was simulated by a cable attenuated by 28 dB, simulating a two way delay of 14 ns. The final two cables represented weaker reflections in the sub-surface. They were attenuated by 58 dB and 78 dB, with simulated two way travel times of 32 ns and 46 ns, respectively.

When taking measurements in the CW mode, the transmitting signal had to be reduced to -31 dBm and the receiver gain had to be reduced by 31 dB in order to avoid clipping the signal in the ADC because of the strong direct signal. In the gated mode, the two strong reflections are removed by setting the τ_{Tx} and τ_{Rx} to 25 ns. The system can then transmit with full power, at 0 dBm, without being saturated because the gating window strongly attenuates the closest reflection while leaving the weaker one almost at full strength. Fig. 8 shows the received magnitude plot together with the gating window. The gain from the gating window has been removed from the gated data. The weakest reflector at 46 ns is buried below the noise in the CW data. This illustrates the gated mode's ability to attenuate close and strong reflectors in order to increase output power and receiver gain. This advantage allows us to remove or reduce the direct wave, as well as the first reflection from the ground, and increase the gain for deeper reflections.

B. Field Test

During 14th - 28th April, 2008, we tested the radar in Engelskbukta near Ny-Ålesund on Svalbard [19].

We mounted the system on a sled pulled by a snowmobile (fig. 9). The case containing the radar and the antennas were attached to a fiberglass pole to reduce reflections from the sled and snowmobile. We mounted the antennas close to the radar, with a cable length of 50 cm, and used a GPS with external antenna to measure the absolute position of the radar. An encoder wheel works as a trigger for the radar, ensuring equidistant samples. The aluminum case contains the GPS, battery for all the equipment and a ruggedized computer running the radar software.

We chose the test site for its unique geological structure. At the base of the Uværsbreen glacier there is an old moraine covered by a layer of ice. During a flood a 2-3 m thick layer of sediments was deposited on top of the ice. Consequently, we hoped to see these internal structures within a penetration of at least three meters. The site had previously been photographed, and surveyed with an 800 MHz impulse radar [20].

We collected several profiles of about 600 m using different modes and parameters. Best results were obtained using the parameters shown in table I. The transmitted power was increased by 31 dB for the gated mode compared to the CW mode. The receiver gain was also increased by 31 dB, giving a total gain of 62 dB. We used the lower gain in the CW mode to avoid saturation of the receiver from the direct wave. The center frequency is 1.75 GHz and the bandwidth is 2.5 GHz. The antenna was approximately 30 cm above the surface and co-polarized.

Dette er en postprint-versjon / This is a postprint version.
DOI til publisert versjon / DOI to published version: 10.1109/TGRS.2011.2160069

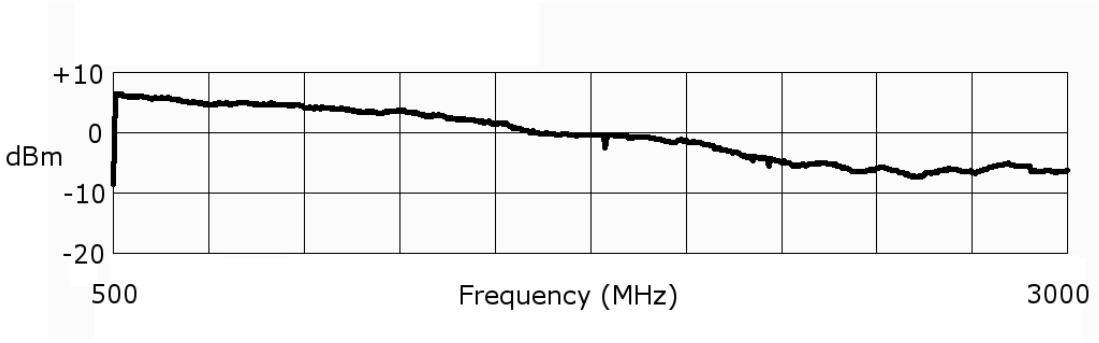

Fig. 6. Measured spectrum fed to the transmitting antenna.

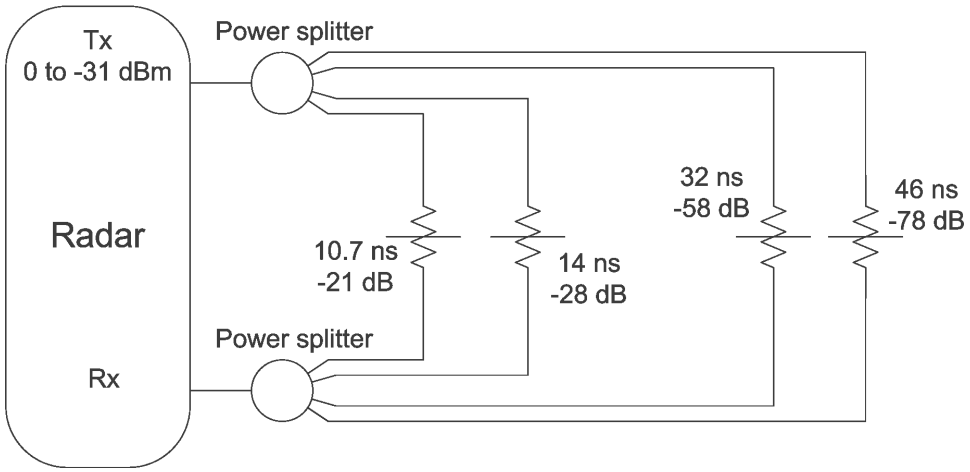

Fig. 7. Test setup using four cables with varying attenuation to simulate a direct wave with 10.7 ns delay and three reflectors with two way travel times of 14 ns, 32 ns and 46 ns.

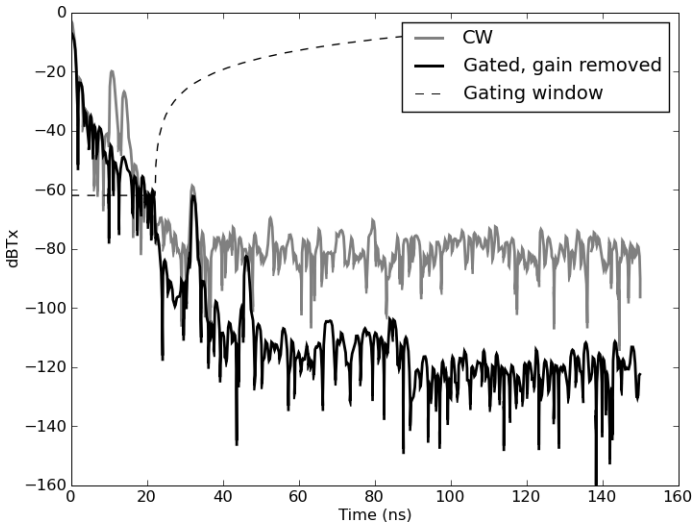

Fig. 8. Measured magnitude plot with the cable test setup for non-gated CW mode in gray, and gated mode in black. The dotted line is the gating window which has been removed from the gated data.

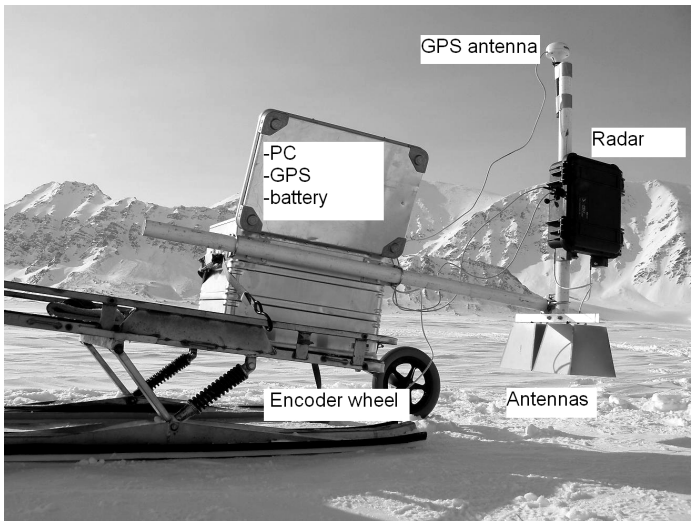

Fig. 9. Radar system set up for field testing.

Fig. 10 and fig. 11 compare the CW and gated versions of the same 120 m profile. For both, the start time was moved by 10 ns and the background was removed with a moving average filter. The plotted profiles consist of 6000 traces and 3672 samples per trace, which gets aliased if plotted in a small figure or on the computer screen. To improve this, the envelope

Dette er en postprint-versjon / This is a postprint version.
DOI til publisert versjon / DOI to published version: 10.1109/TGRS.2011.2160069

of the real part of the data was plotted. For the CW profile, additional gain was applied in the processing to improve the visualization. In the gated data, no additional gain was applied. The surface reflection (1) can be seen in both modes, but is weaker in the gated radar data. There is a varying layer of snow and ice covering the layer of frozen sediments (2). The radar penetrates well into the sediments and the sediment-glacial ice interface can be seen in both radar modes. There are some internal structures of unknown origin (3) which could be in the ice or moraine to the side of the radar. Beneath the ice, the moraine (4) can be seen down to 11 m in the gated mode while disappearing in noise at about 7.5 m in the CW data.

Fig. 12 shows the detail of the upper boxed section in the gated profile of fig. 11. Here, the real value of the radar data is plotted, giving a result comparable to impulse radar. The surface layer of snow 1-1.5 m thick covers the sediments. The sediment layer is about 1.5 m thick here and shows more internal scattering than does the snow above. It is also possible to see internal layers in the sediments. Below the layers of sediment there is old, glacial ice, which has much less scattering than the sediments.

Fig. 13 shows the detail of the lower boxed area of fig 11, with penetration of snow, sediments, and ice. The penetration is 5-8 m deep with the interface between the ice and the old moraine shown on the bottom. There is even some penetration into the moraine. It is possible that the deep penetration occurs because the sediments and moraine are ice rich. The sediments were brought down by freshwater flow which could have washed out salt from the material. This means the sediments could have low conductivity.

V. Conclusions

In this paper, we showed the design and implementation of a prototype for the WISDOM SFCW radar. The antennas do not require contact with the ground. We use range gating, which worked well for short range where the leakage between antennas or strong first reflections limits the dynamic range. The gating frequency must be chosen to include the whole range of interest within the gating window, which could limit the usefulness if looking at long range intervals. The range gating greatly improved system dynamic range compared to CW, both on cable measurements and in the field.

The WISDOM radar prototype worked well and penetrated several meters in the field test site with permafrost sediments and ice, but this does not guarantee penetration in all materials. Future tests could include layered, solid ground with permafrost to test for penetration in other materials than the low conductivity sediments measured in this paper. It should be possible to find moraines with higher salt contents which could be more difficult to penetrate with this radar prototype.

The flight version of the WISDOM radar will do full-polarimetric measurements. Although the antenna used in this paper supported full-polarimetry, the radar hardware did not. For future field tests, this will be implemented and tested. A future version could also have higher transmitter power to further improve system dynamic range, as the radar receiver is not saturated by the current transmitted power in the gated mode.

References

[1] P. Baglioni, R. Fisackerly, B. Gardini, G. Gianfiglio, A. Pradier, A. Santovincenzo, J. Vago, and M. van Winnendael, "The mars exploration plans of esa," *Robotics and Automation Magazine, IEEE*, vol. 13, no. 2, pp. 83–89, June 2006.

[2] J. Taylor, "Ultrawideband radar," *Microwave Symposium Digest, 1991., IEEE MTT-S International*, pp. 367–370 vol.1, Jul 1991.

[3] C.-C. Chen, S. Nag, W. Burnside, J. Halman, K. Shubert, and J. Peters, L., "A standoff, focused-beam land mine radar," *Geoscience and Remote Sensing, IEEE Transactions on*, vol. 38, no. 1, pp. 507–514, Jan 2000.

[4] K. Langley, S. E. Hamran, K. A. Hogda, R. Storvold, O. Brandt, J. O. Hagen, and J. Kohler, "Use of c-band ground penetrating radar to determine backscatter sources within glaciers," *Geoscience and Remote Sensing, IEEE Transactions on*, vol. 45, no. 5, pp. 1236–1246, May 2007.

[5] E. Pettinelli, P. Burghignoli, A. Pisani, F. Ticconi, A. Galli, G. Vannaroni, and F. Bella, "Electromagnetic propagation of gpr signals in martian subsurface scenarios including material losses and scattering," *Geoscience and Remote Sensing, IEEE Transactions on*, vol. 45, no. 5, pp. 1271–1281, May 2007.

[6] M. Hussain, "Ultra-wideband impulse radar-an overview of the principles," *Aerospace and Electronic Systems Magazine, IEEE*, vol. 13, no. 9, pp. 9–14, Sep 1998.

[7] P. Paillou, G. Grandjean, N. Baghdadi, E. Heggy, T. August-Bernex, and J. Achache, "Subsurface imaging in south-central egypt using low-frequency radar: Bir safsaf revisited," *Geoscience and Remote Sensing, IEEE Transactions on*, vol. 41, no. 7, pp. 1672–1684, July 2003.

[8] D. Daniels, *Ground-penetrating radar*, 2nd ed. London: Institution of Electrical Engineers, 2007.

[9] N. Maaref, P. Millot, C. Pichot, and O. Picon, "A study of uwb fm-cw radar for the detection of human beings in motion inside a building," *Geoscience and Remote Sensing, IEEE Transactions on*, vol. 47, no. 5, pp. 1297–1300, May 2009.

[10] A. Meta, P. Hoogeboom, and L. Ligthart, "Signal processing for fmcw sar," *Geoscience and Remote Sensing, IEEE Transactions on*, vol. 45, no. 11, pp. 3519–3532, Nov. 2007.

[11] S. Axelsson, "Frequency and azimuthal variations of radar cross section and their influence upon low-frequency sar imaging," *Geoscience and Remote Sensing, IEEE Transactions on*, vol. 33, no. 5, pp. 1258–1265, Sep 1995.

[12] J. Fransson, F. Walter, K. Blennow, A. Gustavsson, and L. Ulander, "Detection of storm-damaged forested areas using airborne carabas-ii vhf sar image data," *Geoscience and Remote Sensing, IEEE Transactions on*, vol. 40, no. 10, pp. 2170–2175, Oct 2002.

[13] S. E. Hamran, D. T. Gjessing, J. Hjelmstad, and E. Aarholt, "Ground penetrating synthetic pulse radar: dynamic range and modes of operation," *Journal of Applied Geophysics*, vol. 33, no. Issues 1-3, pp. 7–14, January 1995.

[14] S.-E. Hamran, "Radar performance of ultra wideband waveforms," in *Radar Technology, ISBN: 978-953-307-029-2*, G. Kouemou, Ed. In-Tech, 2009.

[15] F. Fois, R. Mecozzi, M. Iorio, D. Calabrese, O. Bombaci, C. Catallo, A. Croce, R. Croci, M. Guelfi, E. Zampolini, D. Ravasi, M. Molteni, P. Ruggeri, A. Ranieri, M. Ottavianelli, E. Flamini, G. Picardi, R. Seu, D. Biccari, R. Orosei, M. Cartacci, A. Cicchetti, A. Masdea, E. Giacomoni, M. Cutigni, M. Provenziani, O. Fuga, G. Alberti, S. Mattei, C. Papa, P. Marras, B. Tattarletti, D. Vicari, F. Bonaventura, T. Paterno, A. Di Placido, and A. Morlupi, "Comparison between marsis and sharad results," *Geoscience and Remote Sensing Symposium, 2007. IGARSS 2007. IEEE International*, pp. 2134–2139, July 2007.

[16] V. Ciarletti, S.-E. Hamran, and C. Corbel, "Instrument information package pasteur instrument payload for the exomars mission," Tech. Rep., April 2006.

[17] M. J. Øyan, S.-E. Hamran, T. Berger, and L. Hanssen, "Characterisation of ultra wideband frequency modulated and step frequency radar with range gating." IASTED, ARP2009, July 2009.

[18] D. Plettemeier, V. Ciarletti, S. E. Hamran, C. Corbel, P. Cais, W.-S. Benedix, K. Wolf, S. Linke, and S. Roddecke, "Full polarimetric gpr antenna system aboard the exomars rover," in *Radar Conference, 2009 IEEE*, May 2009, pp. 1–6.

[19] S. E. Hamran, V. Ciarletti, C. Corbel, D. Plettemeier, M. J. Øyan, T. Berger, and L. Hanssen, "The wisdom shallow sounding gpr on the exomars mission," in *12th International Conference on Ground Penetrating Radar*, June 2008.

Dette er en postprint-versjon / This is a postprint version.
DOI til publisert versjon / DOI to published version: 10.1109/TGRS.2011.2160069

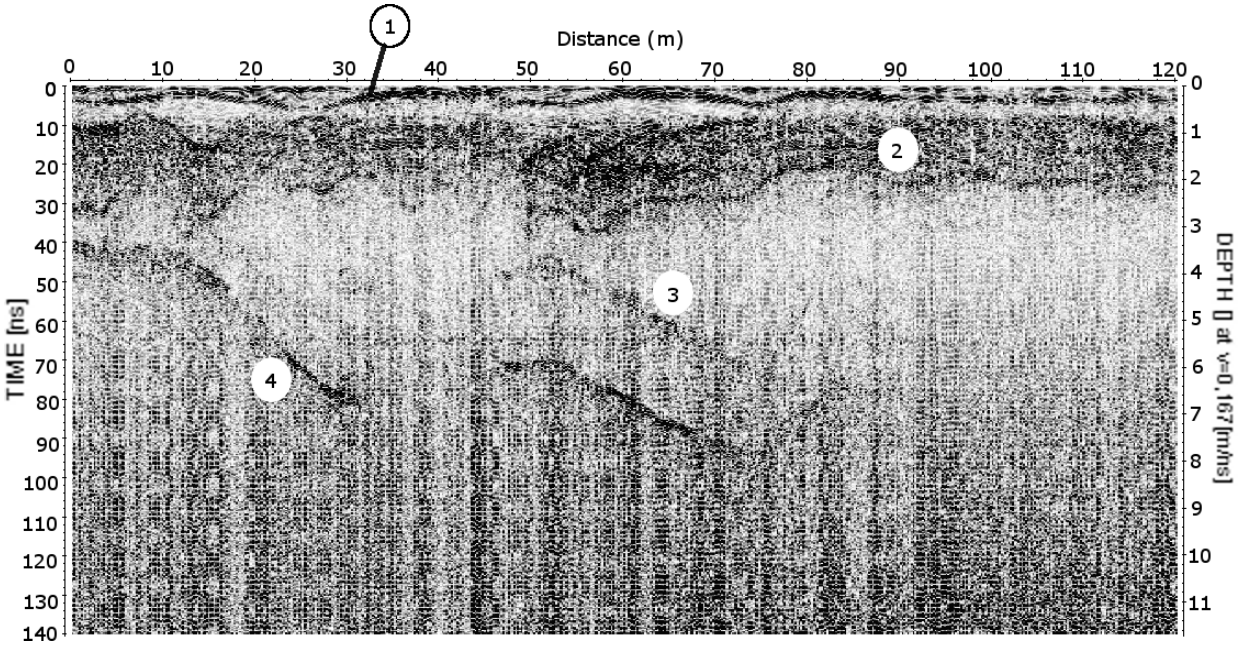

Fig. 10. 120 m long profile in CW mode showing the surface reflection (1), snow, a sediment layer (2), a layer of ice with internal structures (3) and the moraine (4) at the bottom. Post processing for this plot comprised removing the average, adding a gain in the time domain increasing with depth and moving the start time so the direct wave between antennas is at t=0 ns.

[20] S.-E. Hamran, T. Berger, L. Hanssen, M. Oyan, V. Ciarletti, C. Corbel, and D. Plettemeier, "A prototype for the wisdom gpr on the exomars mission," *Advanced Ground Penetrating Radar, 2007 4th International Workshop on*, pp. 252–255, June 2007.

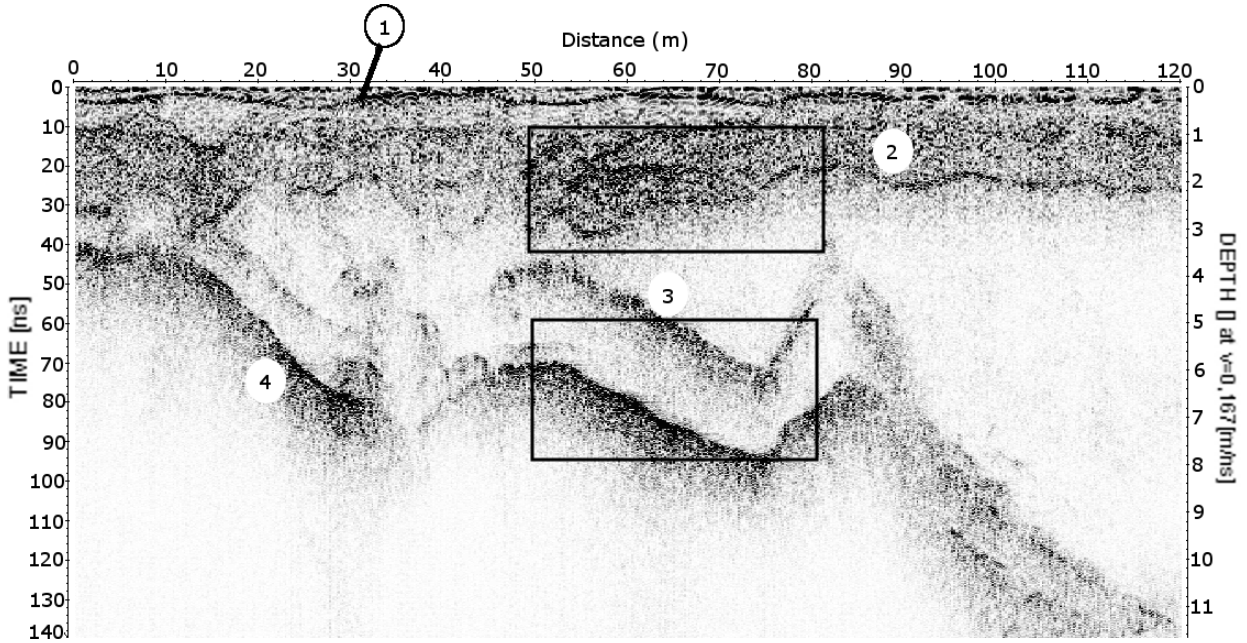

Fig. 11. 120 m long profile in gated mode showing the surface reflection (1), snow, a sediment layer (2), a layer of ice with internal structures (3) and the moraine (4) at the bottom. Penetration to 140 ns can be seen. Post processing for this plot comprised removing average and moving the start time so the direct wave between antennas is at t=0 ns. Because the gating window provides a gain, no additional gain function was needed. Detail within the boxed areas are shown in fig. 12 and fig. 13.

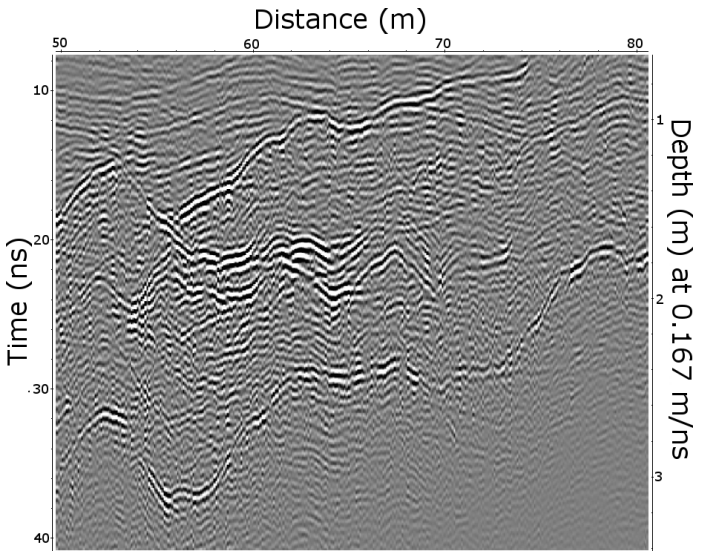

Fig. 12. Detail of boxed part of the gated profile in Fig. 11, which shows the sediments structure.

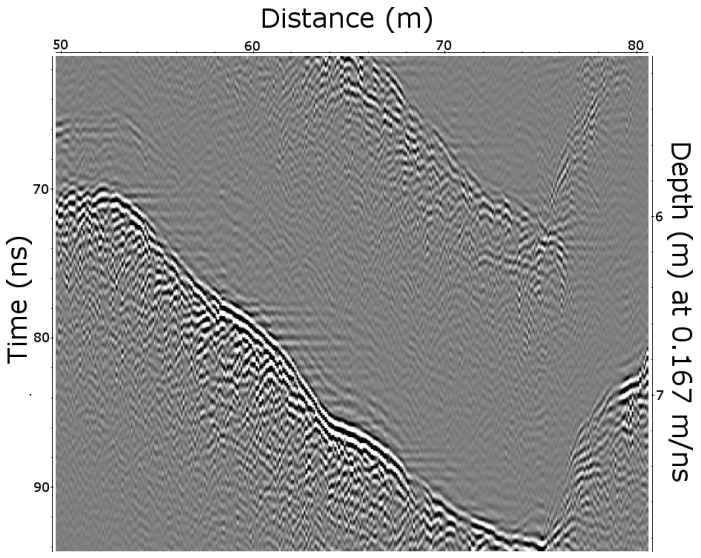

Fig. 13. Detail of lower boxed part of the gated profile in Fig. 11. This shows the ice-moraine interface.

Dette er en postprint-versjon / This is a postprint version.
DOI til publisert versjon / DOI to published version: 10.1109/TGRS.2011.2160069